

Measurement of the initial state gluon radiation using Drell-Yan events at CDF

The CDF Collaboration
URL <http://www-cdf.fnal.gov>

Abstract

This note describes a measurement of the initial state gluon radiation (ISR) in proton-antiproton collisions at $\sqrt{s} = 1.96$ TeV. This analysis uses Drell-Yan ($Z/\gamma^* \rightarrow ee, \mu\mu$) events in the CDF data sample, corresponding to an integrated luminosity of 9.4 fb^{-1} . We find that the mean value of the transverse momentum distribution of the dilepton system is a good observable to measure the effect of the ISR. This observable has a good logarithmic dependence on the mass square of the dileptons, which is parameterized as a linear function of $-7.61 + 2.15 \times \log(M^2)$. The measurement of this observable provides a good way to estimate the effect of the ISR at very high mass region, and it can be used to control the size of the ISR effect in other physics processes.

1 Introduction

Since the discovery of the Higgs boson [1] in 2012, searching for physics beyond the Standard Model (SM) has become the highest priority at hadron colliders. Precise understanding on the SM processes is required to search for any deviation from the SM. However, the SM process with extra jets from initial state gluon radiations (ISR) is difficult to be simulated, especially when extra jets are soft. Thus, we need a clever way to understand the ISR. The good knowledge of the ISR is also crucial in precise measurements of W and top quark masses, because the transverse momentum (p_T) of W or top quark-pair can be mis-modeled. In addition, many interesting signals for the beyond the SM have invisible pair-particles (like dark matters) with mono-jet from initial state gluon radiation. It is important to have a precise understanding on the effect of the ISR.

The initial state gluon radiations from incoming partons in hadron collider are not something in a black box we do not understand. The ISR is basically controlled by the DGLAP evolution equation [2]. This has been studied in lepton-nucleon inelastic scattering experiments. The DGLAP equation tells us that the change in incoming quark distribution, dq due to an ISR is given by

$$\frac{dq(x, Q^2)}{d \log Q^2} = \int_x^1 \frac{dy}{y} \alpha_s \left(\frac{Q^2}{\Lambda_{\text{QCD}}^2} \right) P_{q \rightarrow qg} \left(\frac{x}{y}, Q^2 \right) q(y, Q^2) \quad (1)$$

where $q(y, Q^2)$ is the quark distribution with momentum fraction $y (> x)$, and $P_{q \rightarrow qg}$ is a splitting function, the probability of the quark to split into quark and gluon. Thus, the ISR effect is basically governed by the Q^2 , Λ_{QCD} , and parton distributions functions (PDFs), and splitting functions.

In order to study the effect of the ISR, we need to select event sample with a good knowledge on Q^2 and PDFs and the ISR activity also needs to be isolated in events. However, many SM processes face a challenge to disentangle the ISR activity from the final state gluon radiations (FSR) activity in events. Thus, we use the Drell-Yan events where Z/γ^* decays to leptons ($p\bar{p} \rightarrow Z/\gamma^* \rightarrow ee, \mu\mu$). The Drell-Yan events do not have the FSR activity and has a well defined Q^2 , which is the invariant mass square (M^2) of the dileptons. To explore the ISR activity in the soft QCD region, the Drell-Yan events with transverse momentum of dilepton ($p_T^{\ell\ell}$) less than 100 GeV are used for this measurement.

Since the Q^2 dependence is well controlled by the DGLAP equation, we study the ISR effect by looking at different Q^2 regions. The $p_T^{\ell\ell}$ and number of jets are sensitive to the ISR effect. Figure 1 shows the compatible size of deviation in the $p_T^{\ell\ell}$ distribution due to the 6% variation of α_s for space-like parton shower (parton showering before head-on collisions). It implies that the $\langle p_T^{\ell\ell} \rangle$ is correlated with the ISR activity. The transverse momenta of various physics processes also follow the same logarithmic dependency on the hard process energy scale as shown in the Figure 2, which is understood with the DGLAP equation. When an event is produced with

a higher momentum transfer, the more gluon evolution from the colliding quarks is consequently expected, which makes higher $p_T^{\ell\ell}$.

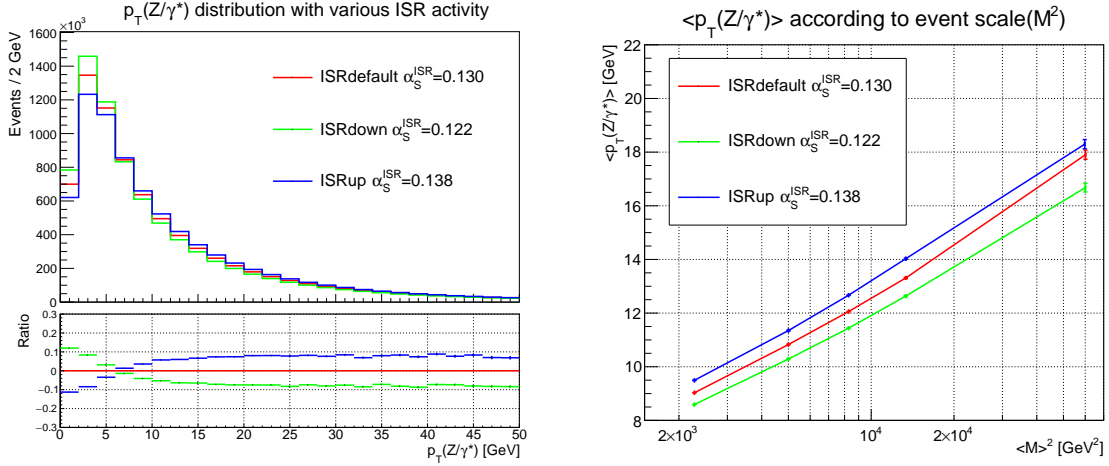


Figure 1: p_T of Drell-Yan simulation sample with various α_S^{ISR}

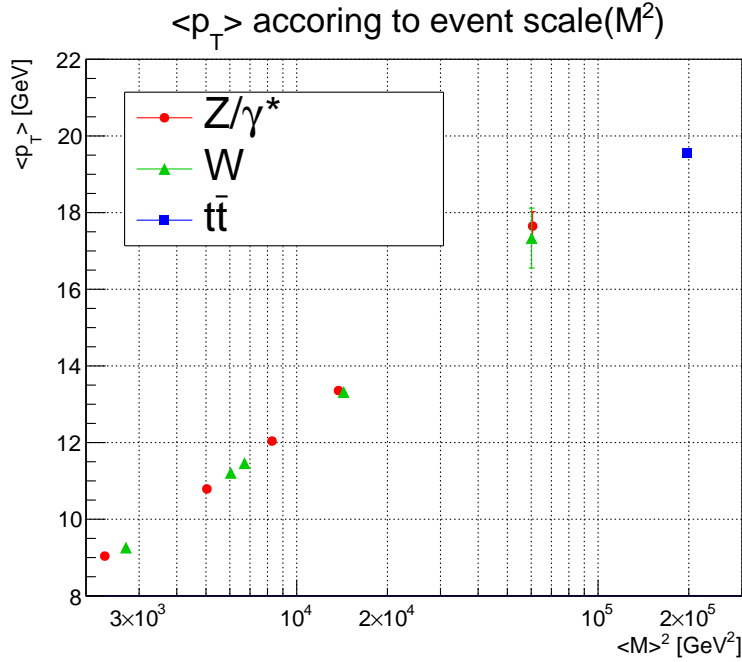


Figure 2: p_T according to event scale

2 Event Selection

The dimuon and dielectron events in Drell-Yan are used for this study. For dimuon events, single muon trigger with a track p_T threshold of 18 GeV is used. For dielectron events, single electron trigger and double e/γ trigger with $E_T > 18$ GeV are used. Selected events are then required to pass each electron and muon criteria in offline. The difference of the acceptance and efficiency between the simulation and data is corrected by applying scale factors to the simulation sample for each channel. The trigger and identification scale factors for electrons are obtained using tag-and-probe method depending on the pseudorapidity, E_T , and number of vertex, and run periods. The scale factors for muon are corrected separately per dimuon topology. The number of vertices and z_0 distribution of the selected events are reweighted following the data profile.

Muon candidate needs to have a matched muon stub except that it falls into the gaps of the muon chambers. A set of quality track cuts and no significant calorimeter energy along with the track are required for the muon selection. For the $\mu\mu$ events, two opposite-signed muons are selected with each muon $p_T > 20, 12$ GeV and $|\eta| < 1.5$.

The electron pair events are obtained in three different topologies: central-central (CC), central-plug (CP), and plug-plug (PP) regions (central/plug means the central/forward electromagnetic calorimeter). In CC Drell-Yan candidates, the central electron candidates are required to have a matched central track with quality cuts and appropriate shower profile. Two electrons should have opposite sign and satisfy $E_T > 25, 15$ GeV in order of p_T . As the central outer tracker cannot cover the forward region, the CP and PP electron pairs have no charge requirement. In CP, central electron criteria are imposed on the central electron leg and both electrons must have $E_T > 20$ GeV. The PP electrons are required to have $E_T > 25$ GeV and decay into same side of calorimeter for the QCD contribution reduction. For the ee candidates imbalance of the transverse energy (\cancel{E}_T) is required to be less than 40 GeV to reduce mis-reconstructed events and background process.

In electron channel, the QED FSR events are difficult to simulate at low M^2 region where its effect is relatively strong due to the migration from Z peak. In order to suppress the migration effects, additional selection cuts are applied to the events with low dielectron mass, $M^{ee} < 80$ GeV, as below:

FSR-suppress cut:

$$\text{Veto if } |\Delta\phi(e1, e2) - \pi| < 0.25 \text{ AND } \begin{cases} \Delta p_T(e1, e2) > 15 \text{ GeV, when } \cancel{E}_T < 15 \text{ GeV} \\ \Delta p_T(e1, e2) > 10 \text{ GeV, when } \cancel{E}_T > 15 \text{ GeV} \end{cases}$$

This analysis focuses on the ISR in softly evolving QCD region. All the selected Drell-Yan candidates are required to have the $p_T^{\ell\ell} < 100$ GeV. This selection cut is chosen to remove backgrounds including mis-reconstructed events based on the simulation study.

3 Estimation of Backgrounds

For muon channel, $Z \rightarrow \tau\tau$, dibosons (WW, WZ, ZZ), $t\bar{t}$, W, and QCD multi-jet processes are included as background processes. They are calculated by Monte Carlo (MC) simulation samples except multi-jet QCD process which is extracted from data. MC simulations are generated by PYTHIA6 and processed by CDF detector simulation. Multi-jet QCD background is obtained using same sign muons data events following the Ref. [3]. Observed and expected Drell-Yan dimuon candidates show a good agreement in the dimuon mass distribution in figure 3. Detailed event yields are listed in table. 1.

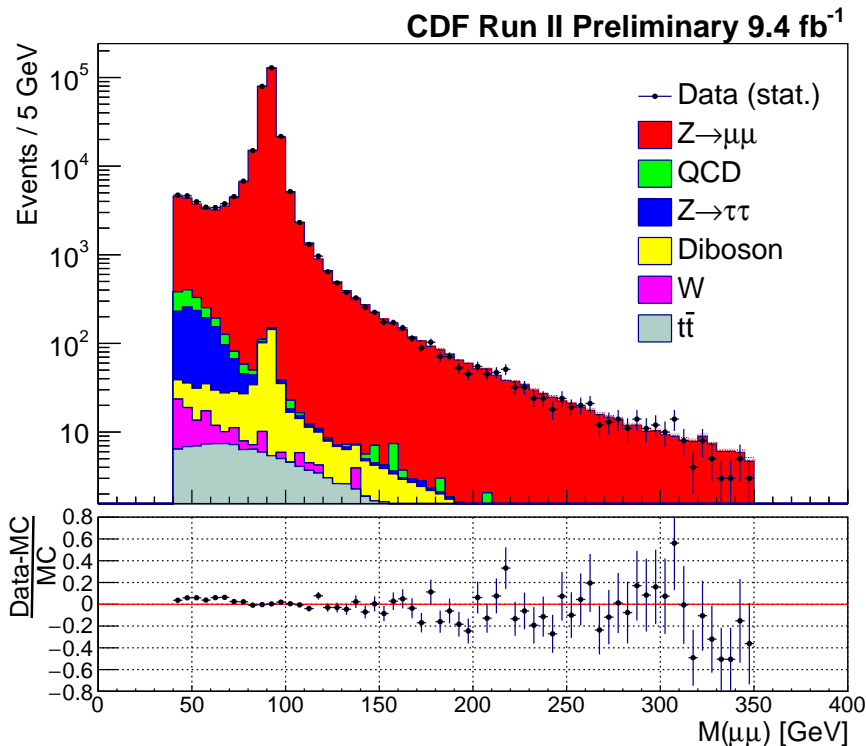


Figure 3: Comparison of dielectron mass distribution between data and MC

For electron channel, $Z \rightarrow \tau^+\tau^-$, dibosons (WW, WZ, ZZ), $t\bar{t}$, W, $W\gamma$, and QCD multi-jet processes are considered as background processes. Like the muon channel, most of them are calculated by MC simulation. The multi-jet QCD events are estimated by inverse electron isolation cuts applied to the data and normalized by a fit on the dielectron mass distribution following the method described in [4] VII.(C). Observed and expected Drell-Yan dielectron candidates are compared in figure 4 and their yields are listed in table 2.

$\mu\mu$ channel		CDF Run II Preliminary 9.4 fb ⁻¹				
Mass bin (GeV)		[40, 60]	[60, 80]	[80, 100]	[100, 200]	[200, 350]
data	Number of Events	16754	18471	244729	13089	562
MC	Number of Events	15975	17786	244248	13184	580
	$Z \rightarrow \mu\mu$	91.45%	97.42%	99.86%	98.99%	97.78%
	QCD	2.82%	0.54%	0.01%	0.09%	0.04%
	$Z \rightarrow \tau\tau$	4.85%	1.40%	0.01%	0.06%	0.02%
	Diboson	0.42%	0.40%	0.12%	0.52%	1.32%
	W	0.29%	0.07%	0.00%	0.04%	0.00%
	$t\bar{t}$	0.17%	0.16%	0.01%	0.31%	0.84%

Table 1: Background contribution in $\mu\mu$ channel

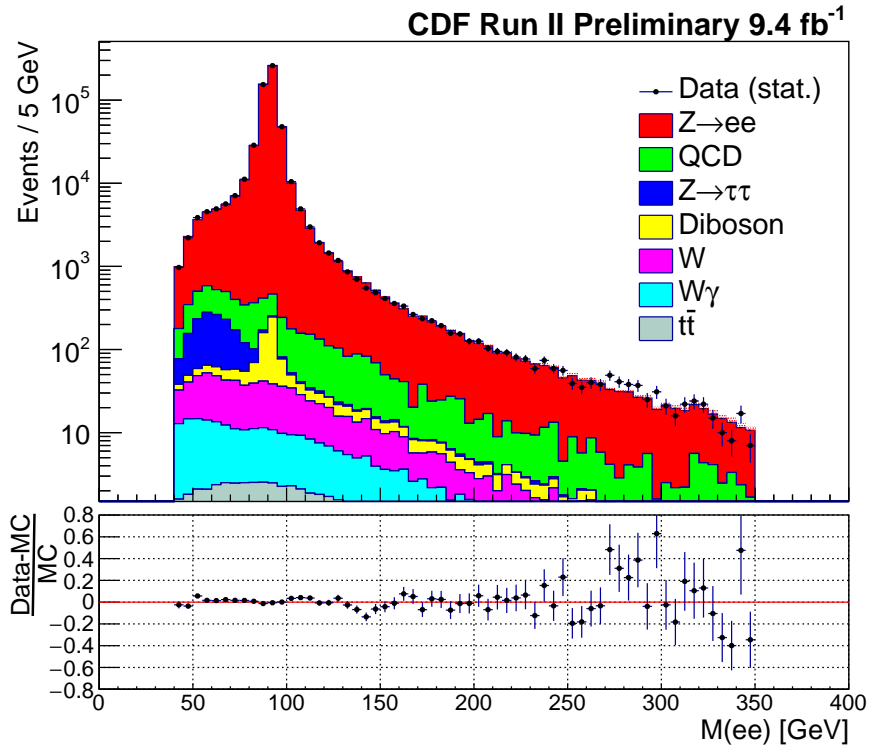


Figure 4: Comparison of dielectron mass distribution between data and MC

<i>ee</i> channel		CDF Run II Preliminary 9.4 fb ⁻¹				
Mass bin (GeV)		[40, 60]	[60, 80]	[80, 100]	[100, 200]	[200, 350]
data	Number of Events	11590	28856	490211	27956	1357
	Number of Events	11416	28374	493391	27481	1307
	Z→ee	85.88%	93.78%	99.70%	94.67%	85.12%
	QCD	7.58%	3.45%	0.18%	3.96%	10.98%
	Z→ττ	4.70%	1.95%	0.01%	0.06%	0.12%
MC	Diboson	0.33%	0.22%	0.08%	0.35%	1.15%
	W	1.03%	0.43%	0.02%	0.62%	1.48%
	Wγ	0.43%	0.13%	0.01%	0.25%	0.87%
	t \bar{t}	0.07%	0.03%	0.00%	0.09%	0.28%

Table 2: Background contribution in ee channel

4 Measurement on the ISR in Drell-Yan events

The observed Drell-Yan events after subtracting background contributions are used for the ISR measurement. In order to understand ISR of data better it is important to have same scale and resolution of the simulated leptons with the measured one in data. Thus we apply energy and momentum correction to the simulation. The corrections of momentum scale and resolution described in [5] are applied to simulated muons depending on the track curvature, pseudorapidity, and azimuthal angle. Electron corrections for scale and resolution are obtained and applied in a similar manner with muons.

The $p_T^{\ell\ell}$ is determined by ISR activity. Parton shower algorithm in PYTHIA6 uses soft-collinear approximation to calculate ISR. This is fast and efficient but has restricted precision at leading logarithm order, which causes the discrepancy in the $p_T^{\ell\ell}$ between data and MC due to higher order effect. Mis-tuning of beam remnant Kt also leads to this disagreement. The MC simulation events are reweighted depending on the boson p_T at generator level.

This correction for electron channel and muon channels should be same because it is generator level correction which is independent on lepton flavor. The correction is extracted iteratively from reconstruction level using both dielectron and dimuon events at Z peak region, 66–116GeV, as a function of p_T and rapidity of the boson. We parameterize the correction with piece-wise polynomial function for p_T in log scale and with simple linear function for pseudorapidity. After boson p_T correction, $p_T^{\ell\ell}$ at reconstruction level shows a good agreement between data and MC in figures 5.

The $\langle p_T(Z/\gamma^*) \rangle$ at truth level is obtained by applying another corrections for the detector effect and QED FSR to the reconstruction level $\langle p_T^{\ell\ell} \rangle$. The correction is determined by the ratio $\langle p_T(Z/\gamma^*) \rangle$ to $\langle p_T^{\ell\ell} \rangle$ as shown in equation 2 based on the Drell-Yan

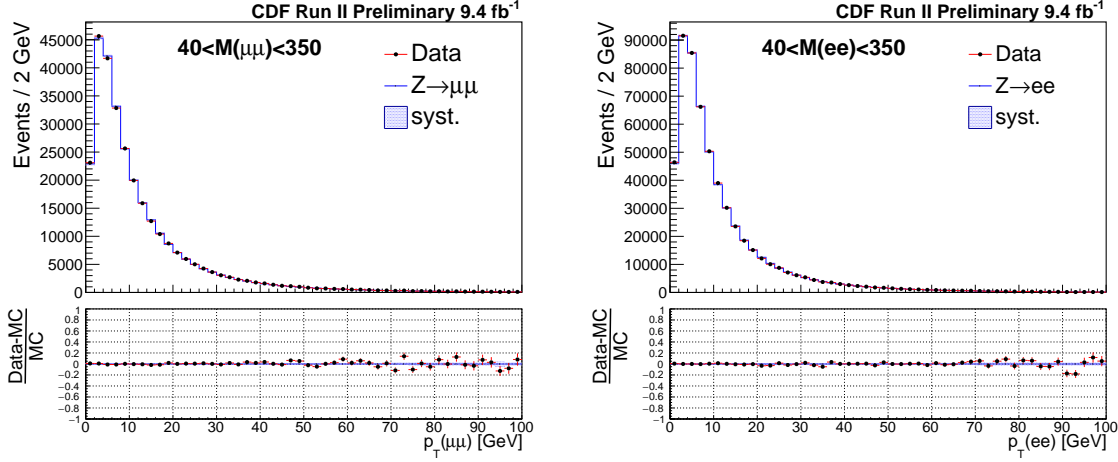


Figure 5: $p_T^{\ell\ell}$ after correcting the p_T distribution for both ee and $\mu\mu$ channel

simulation sample and called a correction factor \mathcal{R} . Here the $\langle p_T(Z/\gamma^*) \rangle$ is the mean of $p_T(Z/\gamma^*)$ at a full-phase-space generator level and $\langle p_T^{\ell\ell} \rangle$ is the mean of $p_T^{\ell\ell}$ at reconstruction level in the MC simulation. For both $p_T(Z/\gamma^*)$ and $p_T^{\ell\ell}$ high-end p_T cut on dilepton is applied. The mean of $M^{\ell\ell}$ at each mass bin also corrected same way as shown in equation 3.

$$\langle p_T(Z/\gamma^*) \rangle_{\text{data}} = \mathcal{R}_{p_T} \times \langle p_T^{\ell\ell} \rangle_{\text{data}} \quad (2)$$

$$\text{where } \mathcal{R}_{p_T} \equiv \frac{\langle p_T(Z/\gamma^*) \rangle_{\text{MC}}^{\text{Generator}}}{\langle p_T^{\ell\ell} \rangle_{\text{MC}}^{\text{Detector}}}$$

$$\langle M(Z/\gamma^*) \rangle_{\text{data}} = \mathcal{R}_M \times \langle M^{\ell\ell} \rangle_{\text{data}} \quad (3)$$

$$\text{where } \mathcal{R}_M \equiv \frac{\langle M(Z/\gamma^*) \rangle_{\text{MC}}^{\text{Generator}}}{\langle M^{\ell\ell} \rangle_{\text{MC}}^{\text{Detector}}}$$

In figure 6 the $\langle p_T^{\ell\ell} \rangle$ dependence on $\langle M^{\ell\ell} \rangle^2$ shows difference tendency in reconstruction level. Due to different detector coverage and responses, various lepton p_T selections, and QED FSR. Measured $\langle p_T^{\ell\ell} \rangle$ and $\langle M^{\ell\ell} \rangle$ are corrected to the generator level with the correction factor \mathcal{R} for each lepton channel. The $\langle p_T(Z/\gamma^*) \rangle$ shows a good linear dependency on the logarithmic $\langle M(Z/\gamma^*) \rangle^2$.

5 Systematic Uncertainties

Several systematic sources are considered to make changes in the derivation of correction factor \mathcal{R} from the $\langle p_T^{\ell\ell} \rangle$ and $\langle M^{\ell\ell} \rangle$ and the shifts of mean values. We concern the effects on the analysis from ISR model, QED FSR model, energy/momentum correction, and background normalization. Systematic uncertainties on the mean p_T are listed in table 3 and 4. The uncertainty from ISR model and QED FSR model are dominant.

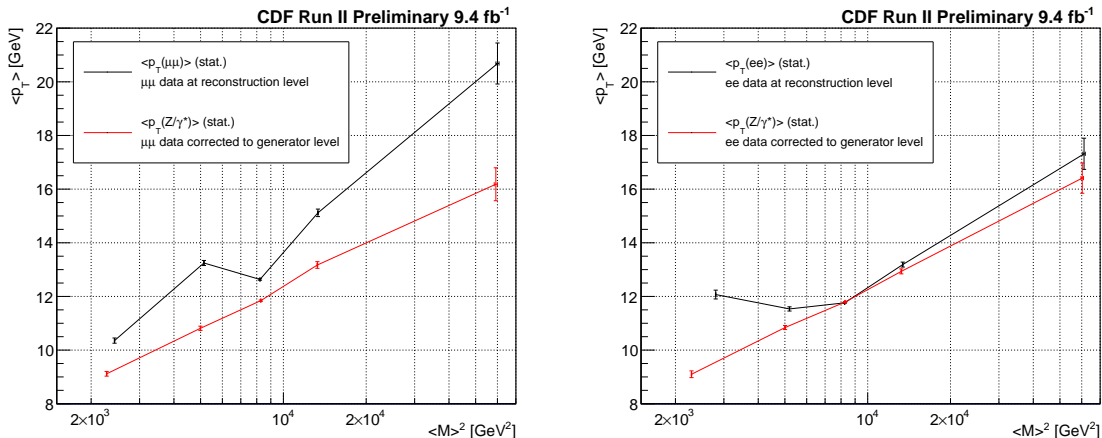


Figure 6: $\langle p_T \rangle$ versus $\langle M \rangle^2$ before and after applying the correction factor \mathcal{R} for $\mu\mu$ (left) and ee (right) events

For the better understanding of data, the $p_T^{\ell\ell}$ distribution is reweighted by boson p_T correction to match the p_T distribution from data. We call the uncertainty coming from this boson p_T correction as the ISR model uncertainty. Two uncertainty sources are considered: the first one is that the boson p_T correction was derived from Z peak events which may cause deviations in other mass bin; the second one is statistical error of boson p_T correction. The uncertainty for ISR model is calculated with pseudo-experiments on various boson p_T corrections considering these two sources. Because we measure mean of $p_T(Z/\gamma^*)$, the systematic uncertainty from boson p_T covers all uncertainty at generator level except QED FSR model.

The simulation we used to extract correction factor \mathcal{R} is generated by PYTHIA6 which calculates FSR with shower algorithm. That algorithm uses a soft-collinear approximation and its precision is leading log order. It could be inaccurate with hard QED radiation. To estimate systematic uncertainty from QED FSR, we compare the generator level result between PYTHIA6 and PHOTOS++. PHOTOS++ calculate multi-photon radiation by iterating single photon radiation of $O(\alpha_{EM})$. We compared the $\langle p_T(Z/\gamma^*) \rangle$ and $\langle M(Z/\gamma^*) \rangle$ at generator level before and after QED FSR both of PYTHIA6 and PHOTOS++ prediction. We take the difference as systematic uncertainty from QED FSR.

The systematic uncertainty from energy/momentum scale is estimated by pseudo-experiments. Each pseudo-experiment is executed with various scale corrections within its statistical uncertainty. For systematic uncertainty from energy/momentum resolution, we changed the parameter controlling additional smearing to MC by a magnitude of the variation determined by χ^2 test with $M(\ell\ell)$ mass distribution between data and MC simulation.

The uncertainty from background is estimated by changing normalization of background process. The factorization/renormalization scale and PDF uncertainty is con-

sidered as uncertainty from cross-section. A total of 6% of data luminosity uncertainty is also considered. Conservatively, we treat the background normalizations are 100% correlated.

$\mu\mu$ channel	CDF Run II Preliminary 9.4 fb ⁻¹				
Mass bin (GeV)	[40, 60]	[60, 80]	[80, 100]	[100, 200]	[200, 350]
Statistical Error(%)	0.96	0.73	0.22	0.95	3.79
Systematic Error(%)	1.31	1.33	0.26	0.91	2.84
ISR model	0.93	0.93	0.24	0.52	2.38
QED FSR	0.87	0.93	0.03	0.18	0.41
Momentum Scale	0.11	0.13	0.04	0.20	0.85
Momentum Resolution	0.07	0.06	0.08	0.68	1.20
Background	0.28	0.10	0.03	0.16	0.25

Table 3: Systematic uncertainties in muon channel

ee channel	CDF Run II Preliminary 9.4 fb ⁻¹				
Mass bin (GeV)	[40, 60]	[60, 80]	[80, 100]	[100, 200]	[200, 350]
Statistical Error(%)	1.38	0.70	0.16	0.72	3.44
Systematic Error(%)	1.96	0.91	0.17	0.63	1.67
ISR model	1.26	0.51	0.13	0.15	1.07
QED FSR	1.39	0.72	0.05	0.22	0.67
Energy Scale	0.11	0.07	0.02	0.08	0.21
Energy Resolution	0.02	0.02	0.08	0.10	0.15
Background	0.57	0.21	0.03	0.56	1.06

Table 4: Systematic uncertainties in electron channel

6 Result

The mean of $p_T(Z/\gamma^*)$ shows logarithmic dependency on M^2 in figure 7. Both $\mu\mu$ and ee channels show consistent result. We perform a linear fit on the results combining both channels, which is $(-7.61 \pm 0.69) + (2.15 \mp 0.08) \times \log M^2$, where M is mass of Z/γ^* divided by 1 GeV. And the unit of parameters are GeV. Two fit parameters are turned out to be strongly anti-correlated by -99.95%. The fit result with muon channel only is $(-7.78 \pm 0.92) + (2.18 \mp 0.10) \times \log M^2$, and the result with electron channel is $(-7.58 \pm 1.04) + (2.15 \mp 0.12) \times \log M^2$. The fit result agree with each other within the uncertainty whether it is performed individually or simultaneously. Each data point in the is also listed at table 5 and 6.

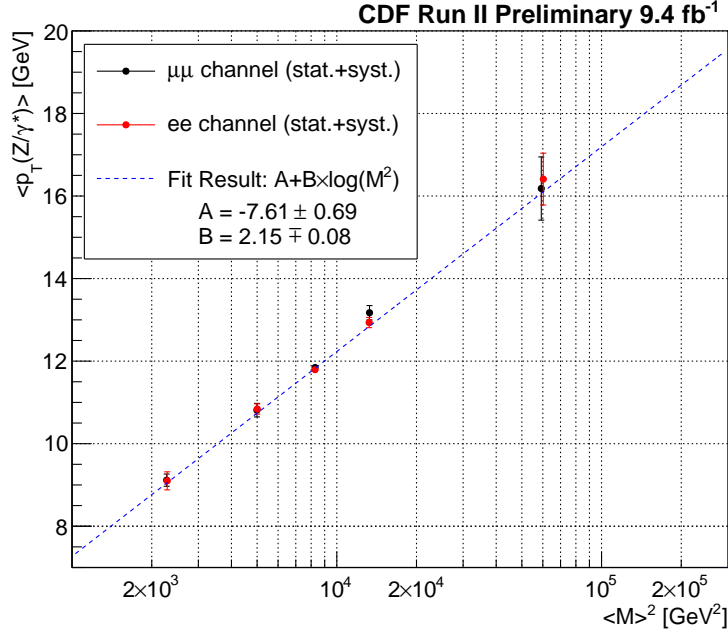


Figure 7: $\langle p_T(Z/\gamma^*) \rangle$ vs M_{Z/γ^*}^2

$\mu\mu$ channel		CDF Run II Preliminary 9.4 fb ⁻¹	
Mass bin	$\langle M \rangle \pm \text{stat.} \pm \text{syst.}$	$\langle p_T(Z/\gamma^*) \rangle \pm \text{stat.} \pm \text{syst.}$	
[40, 60]	47.72 ± 0.05 ± 0.04	9.12 ± 0.09 ± 0.12	
[60, 80]	70.66 ± 0.04 ± 0.07	10.81 ± 0.08 ± 0.14	
[80, 100]	90.99 ± 0.01 ± 0.08	11.84 ± 0.03 ± 0.03	
[100, 200]	115.29 ± 0.18 ± 0.14	13.17 ± 0.12 ± 0.12	
[200, 350]	243.33 ± 1.63 ± 0.41	16.18 ± 0.61 ± 0.46	

(GeV)

Table 5: Muon Channel Result

ee channel		CDF Run II Preliminary 9.4 fb ⁻¹	
Mass bin	$\langle M \rangle \pm \text{stat.} \pm \text{syst.}$	$\langle p_T(Z/\gamma^*) \rangle \pm \text{stat.} \pm \text{syst.}$	
[40, 60]	47.83 ± 0.05 ± 0.07	9.10 ± 0.13 ± 0.18	
[60, 80]	70.76 ± 0.04 ± 0.04	10.84 ± 0.08 ± 0.10	
[80, 100]	90.98 ± 0.01 ± 0.07	11.79 ± 0.02 ± 0.02	
[100, 200]	115.11 ± 0.13 ± 0.14	12.93 ± 0.09 ± 0.08	
[200, 350]	245.46 ± 1.29 ± 0.36	16.41 ± 0.56 ± 0.27	

(GeV)

Table 6: Electron Channel Result

7 Conclusion

The ISR activity is measured using Drell-Yan events in proton-antiproton collisions at $\sqrt{s} = 1.96$ TeV at CDF. We find the measured average value of dilepton p_T shows a good linear dependency on the logarithmic scale of M^2 . The slope is measured to be 2.15 ± 0.08 GeV. This ISR activity occurs universally in the hadron collisions, thus many other analysis like precision measurement and new particle search can take benefit from our result to constrain the effect of ISR. Because its simple logarithmic dependency, the effect of ISR at very high mass region can be obtained easily by extrapolation of the result. It will give smaller uncertainty from ISR than using theoretical uncertainty which have scale ambiguity.

References

- [1] CMS Collaboration, "Observation of a new boson at a mass of 125 GeV with the CMS experiment at the LHC", Phys. Lett. B 716 (2012); ATLAS Collaboration, "Observation of a new particle in the search for the Standard Model Higgs boson with the ATLAS detector at the LHC", Phys. Lett. B 716 (2012)
- [2] Dokshitzer, Y. L. (1977). Yu. L. Dokshitzer, Sov. Phys. JETP 46, 641 (1977). Sov. Phys. JETP, 46, 641; V.N. Gribov, L.N. Lipatov, Sov. J. Nucl. Phys. 15, 438, 675 (1972); L.N. Lipatov, Sov. J. Nucl. Phys. 20, 95 (1975); Altarelli, Guido, and Giorgio Parisi. "Asymptotic freedom in parton language." Nuclear Physics B 126 (1977)
- [3] CDF Collaboration, "Indirect measurement of $\sin^2 \theta_W$ (or M_W) using $\mu^+ \mu^-$ pairs from γ^*/Z bosons produced in $p\bar{p}$ collisions at a center-of-momentum energy of 1.96 TeV", Physical Review D 89 (2014)
- [4] CDF Collaboration, "Measurement of $\sin^2 \theta_{\text{eff}}^{\text{lept}}$ using $e^+ e^-$ pairs from γ^*/Z bosons produced in $p\bar{p}$ collisions at a center-of-momentum energy of 1.96 TeV.", Physical Review D 93 (2016)
- [5] Bodek, Arie *et al.*, "Extracting muon momentum scale corrections for hadron collider experiments.", The European Physical Journal C 72 (2012)